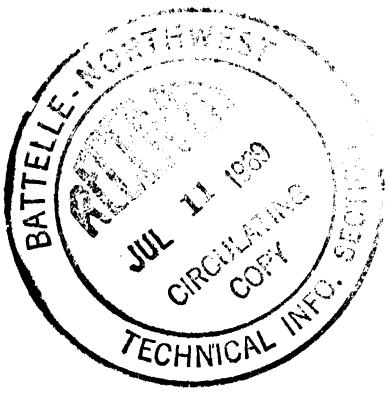

BNWL-1102 DRI
Draft Issue No. 1
May 29, 1969

2 —

U.K. COMMERCIAL DATA EMPLOYED IN FFTF FUEL PIN AND SUBASSEMBLY CONCEPTUAL DESIGN*

E. G. Stevens
P. D. Cohn
R. J. Jackson
D. C. Kolesar
C. L. Mohr
A. Padilla
C. L. Wheeler

Draft Issue Document

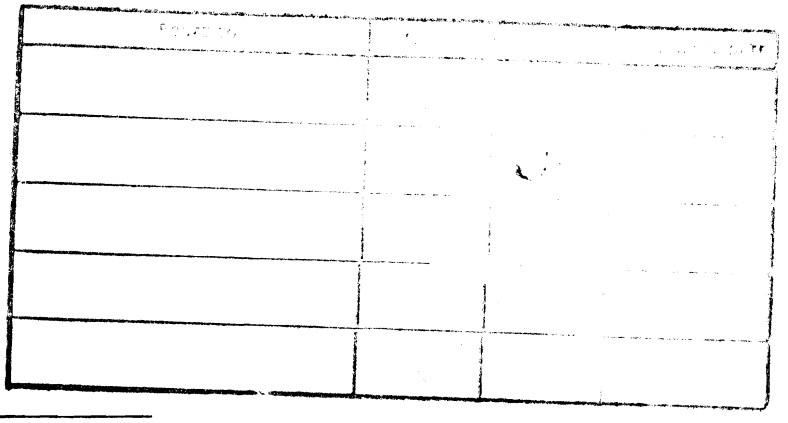

* This document supplements BNWL-1064, FFTF Fuel Pin and Subassembly Conceptual Design Methods and Data

BATTELLE MEMORIAL INSTITUTE
PACIFIC NORTHWEST LABORATORY
RICHLAND, WASHINGTON 99352

INFORMATION CONCERNING USE OF THIS REPORT

PATENT STATUS

This document copy, since it is transmitted in advance of patent clearance, is made available in confidence solely for use in performance of work under contracts with the U. S. Atomic Energy Commission. This document is not to be published nor its contents otherwise disseminated or used for purposes other than specified above before patent approval for such release or use has been secured, upon request, from the Chief, Chicago Patent Group, U. S. Atomic Energy Commission. 9800 So. Cass Ave., Argonne, Illinois.

PRELIMINARY REPORT

This report contains information of a preliminary nature prepared in the course of work under Atomic Energy Commission Contract AT(45-1)-1830. This information is subject to correction or modification upon the collection and evaluation of additional data.

LEGAL NOTICE

This report was prepared as an account of Government sponsored work. Neither the United States, nor the Commission, nor any person acting on behalf of the Commission:

A. Makes any warranty or representation, expressed or implied, with respect to the accuracy, completeness, or usefulness of the information contained in this report, or that the use of any information, apparatus, method, or process disclosed in this report may not infringe privately owned rights; or

B. Assumes any liabilities with respect to the use of, or for damages resulting from the use of any information, apparatus, method, or process disclosed in this report.

As used in the above, "person acting on behalf of the Commission" includes any employee or contractor of the Commission, or employee of such contractor, to the extent that such employee or contractor of the Commission, or employee of such contractor prepares, disseminates, or provides access to, any information pursuant to his employment or contract with the Commission, or his employment with such contractor.

The data contained in this document is passed under the terms of the UKAEA/USAEC Fast Reactor Agreement. Information contained in the document may be used, within the USA, for furtherance of the Fast Reactor Programme or for other purposes as the USAEC may approve. The document or its contents may be made available by the recipient only to contractors of the USAEC engaged in the program or to other parties authorized by USAEC, excluding nationals (other than full-time employees of authorized recipients) of countries other than the U.S. or U.K.

TABLE OF CONTENTS

BNWL-1102
Draft Issue No. 1
May 29, 1969

U.K. COMMERCIAL DATA EMPLOYED IN FFTF FUEL PIN AND SUBASSEMBLY CONCEPTUAL DESIGN

A. FUEL ELEMENT AND SUBASSEMBLY STRUCTURAL BEHAVIOR*

A.1 FUEL AND CLADDING SWELLING IRRADIATION EFFECTS

Fuel Swelling and temperature-burnup effects are being investigated in the Irradiation Programs which include fuel swelling rate, gas release rate, direction of swelling, cladding restraint, etc. The cladding properties for various irradiation exposures and temperatures is extremely important and is discussed in detail.[1,2] Present design is predicated on swelling being accommodated internally up to about 40,000 MWd/tonne. After 40,000, the diametral growth of the pin is manifest externally and must be accommodated within the subassembly.

The fuel pin design from diametral growth viewpoint must be concerned with its relationship to the subassembly. The fuel pins are spirally wrapped with spacer wire and then assembled into a hexagonal bundle, fixed at one end with a grid spacer. Clearances between the wires and the adjacent fuel pins are small. During irradiation, the fuel pin diameter increases. In general, this diameter increase may consist of two components: One component is clad swelling and the other, if present, is mechanical strain in the clad resulting from the fuel swelling. This increased mechanical strain causes an increase in spacer wire tension. This in turn causes a larger spiral deflection of the fuel pin. Because all pins are in a similar environment, the pins will have a similar spiral deformation. Therefore, the entire pin bundle will have a spiral deformation pattern. This

---

* *Contains U.K. Commercial Data*

spiral deformation pattern of the bundle causes the spacer wires to move away from duct wall at the particular elevation where the spacer wire is between the duct wall and a fuel pin. Therefore, the increased mechanical strain causes a net decrease in the bundle envelope. This is offset slightly by the clad swelling component which causes an increase in bundle envelope. The duct also experiences metal swelling and will increase in dimension with increasing fluence. Since the duct wall is colder than the cladding and spacer wires, the duct may swell at a slower rate than the pin bundle. It is possible for the pin bundle envelope to gradually use up the assembly clearance between the pin bundle and duct. The present swelling models predict this will occur at approximately 80,000 MWd/tonne burnup of peak pins. If credit is taken for the deflection of the pins, this packing does not occur. As soon as this increase in bundle envelope exceeds the clearance between the wire and fuel pin, the fuel pin is forced to move sideways. Since the wire wrap is spiral, the movement is spiral along the axis of the pin, resulting in additional spiral bending in the fuel cladding.

Figure A.1-1 shows the FTR fuel pin diameter increase along the fuel column length based upon empirical relationships from U.K. data for solution treated clad. It should be noted that peak pins may have diametral growth of 3% and not at the hottest location on the pin length. Figure A.1-2 shows this bending on fuel pins mocked up to illustrate the effect of spiral bending from diameter increase in a tight duct. These pins were assembled into a bundle, heated, then internally pressurized. Calculations indicate fiber stresses from bending of $\sim$30,000 psi if no stress relaxation is considered.

It is assumed the condition described (bending in a tight duct) can result in or contribute to fuel cladding failure and is therefore undesirable. Consequently, the less fuel cladding

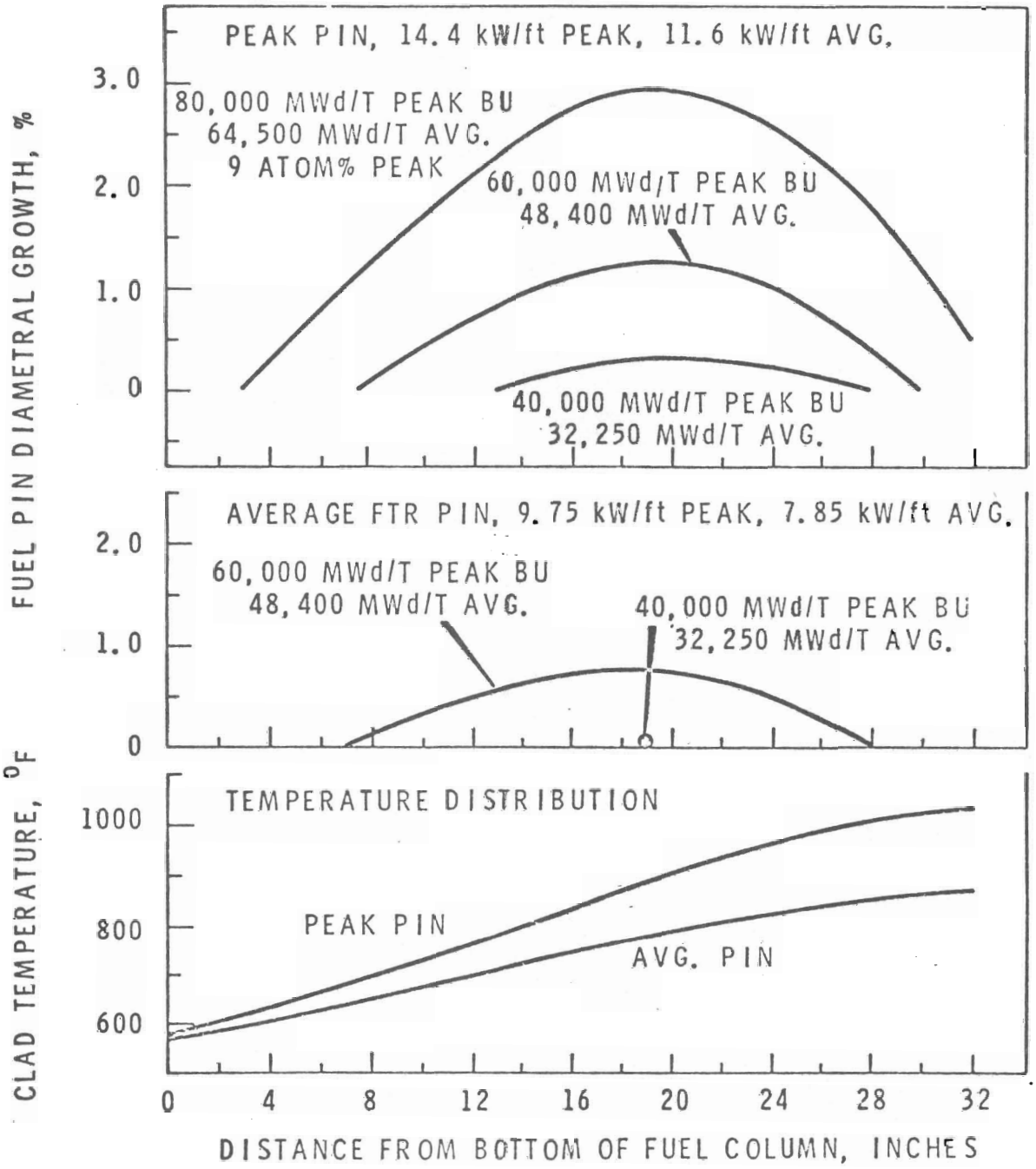

FIGURE A.1-1. FTR Pin Diameter Increase Based Upon Empirical U.K. Relationship Between Temperature and Burnup and then Adjusted for Differences in Clad Fluence

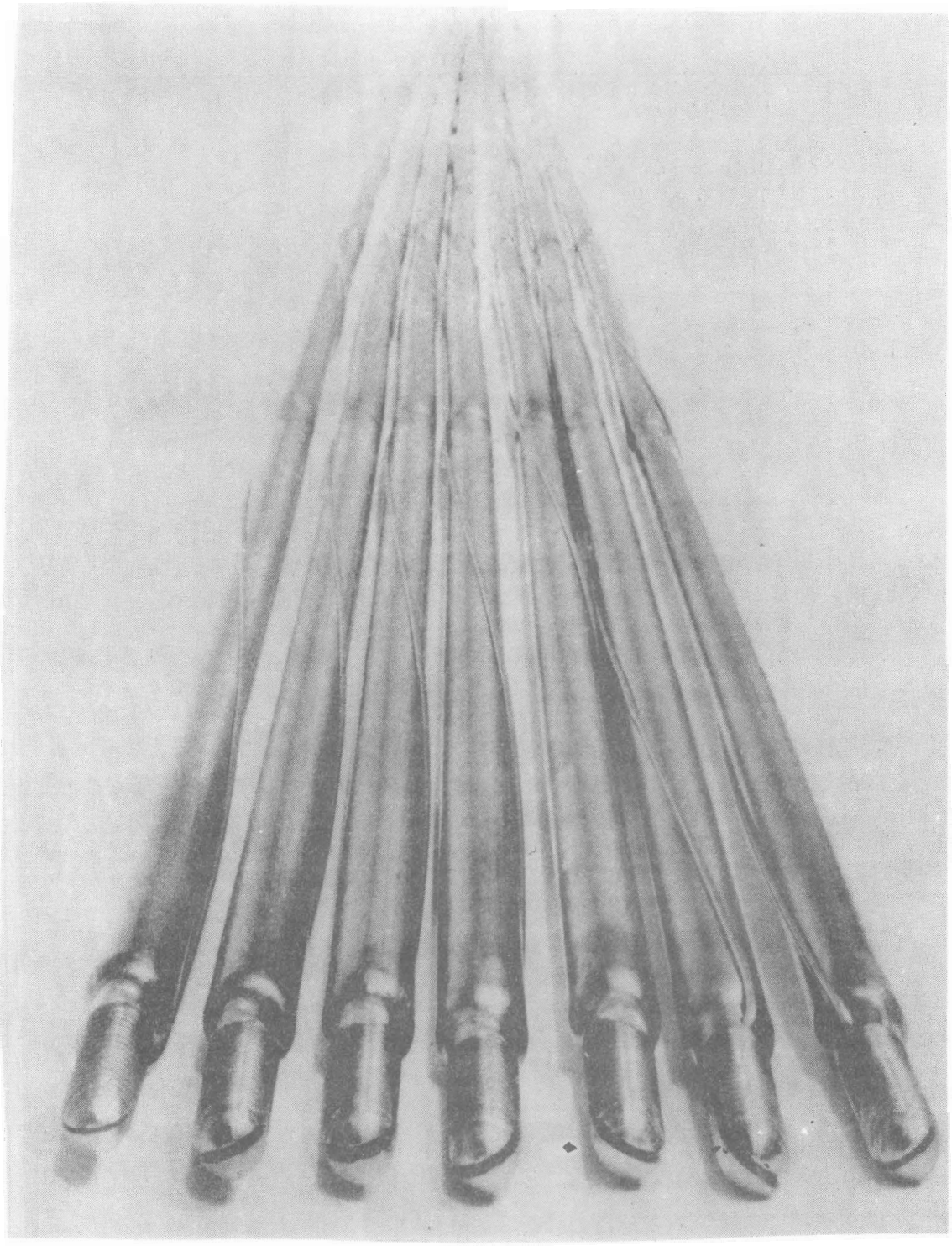

FIGURE A.1-2. Effect of Swelling Upon Pin Bundle Behavior

diameter increase, the less the probability of fuel pin bending occurring. The following shows that cold-worked cladding results in less total diametral growth than does solution annealed cladding. This consideration would indicate a preference for cold-worked cladding for the FTR.

A.1.1 Fuel Irradiation Experience

Of all experience pertaining to stainless steel cladding irradiated in fast reactor environments, at present the most applicable to the FTR are the UKAEA experiments. The French, Russians and the U.S. each have had some applicable experience. However, the French have merely followed the lead of the British and have not completed experiments to the point of having reported data at burnup of interest. The Russians have not reported the details of their cladding experience in sufficient detail to enable our evaluation. U.S. efforts have been small and primarily on Type 304. The British experience has been with M316, which, while modified, is still essentially 316, and major emphasis must be given to their experience.

The British irradiations program[3] consisted of two basic parts: clad fuel pins and subassemblies, and mechanical testing specimens. Results of the latter were discussed under the section in this report on mechanical properties.

The British fuel pin irradiation program consisted of both single pins and subassemblies of pins. The single pin irradiations occurred first in the program, and results were used to design the subassembly experiments. These consisted of a rhombus-shaped wrapper approximately 30 in. long, containing 77 fuel pins in grids at 2-in. intervals along the pins. The pins were 0.230 in. OD by 0.200 in. ID. The cladding was M316 and M316-L, and both solution annealed and

cold-worked conditions were represented. The fuel was mixed oxide containing either 15 or 25% plutonium oxide with the remainder uranium oxide. Most of the fuel was the 15% plutonium oxide variety.

Coolant inlet temperature was approximately 520 °F with most of the subassemblies having outlet temperatures about 1100 °F, with some as high as 1200 °F.

Eight subassemblies have been irradiated, but data has been made available on only the first four to date. These were designated the Mark I, IB, II and IIA. Mark IIB and IIC have been irradiated but no details of these irradiations have been made available. No information is available on the Mark IID and Mark III subassemblies.

The Mark I and IB subassemblies contained both cold-worked and annealed cladding. Some of the cold-worked clad pins had VIPAC fuel, others annular pellets. The same is true for the annealed cladding pins. M316L was used as the cladding material. The Mark II subassembly used all M316 cladding, cold-worked, and contained both VIPAC and annular pellet fuel. The Mark IIA subassembly used cold-worked and annealed M316 and both VIPAC and annular pellet fuel.

In this discussion, there are two key characteristics by which fuel pins are evaluated: (1) Did the cladding fail by splitting or cracking? (2) What was the pattern of diameter increases?

There have been six reported pin failures on the U.K. irradiation program (Table A.1-1). Three of the failures occurred in solution treated cladding, two in "as received" cladding, and one in cold-worked cladding. However, these pins operated under such a variety of conditions that it is invalid to attempt to draw conclusions. None of these operated in the flowing sodium subassemblies but were in stagnant sodium trefoil assemblies.

TABLE A.1-1. Failed Pin Summary, DFR

Fuel Pin Number	Pin Description, in.	Clad Material	Maximum Burnup, %	%Δ Diam	Clad Temp, °C	Failure
CV 002	28 x 0.2 ID VIPAC Carbide	M316L AR[a]	8.0	1.9	570	1 Transverse Crack[b] 5 Longitudinal Cracks
CA 003	28 x 0.275 ID Annular Carbide	M316L AR[a]	5.8	1.4	620	2 Longitudinal Cracks[b]
A 153	28 x 0.2 ID Annular Oxide	M316 CW[c]	9.1	1-2[d]	625	3 Prominent Longitudinal Cracks[e]
V 024	7 x 0.2 ID VIPAC Oxide	M316L ST[c]	7.1	∿4[d]	700 (Est 750-800 °C)	Short Long Cracks[e] 2 in. Long
V 021	7 x 0.2 ID VIPAC Oxide	M316L ST[c]	8.1	∿1/2-6[d]	655 (Est High Oper. Temp)	Several Cracks ∿0.4[e]
V 035[f]	28 x 0.200 ID VIPAC Oxide	M316L ST[c]	6.9	0.7	560	Possible Failure[c]

(a) TRG 3124, Table I
(b) TRG 3124, p. 2
(c) TRG 2942, Table II
(d) TRG 2942, Table VII
(e) TRG 2942, p. 6
(f) TRG 2942, p. 18

The diameter changes for the Mark I and IB do show a trend. Figure A.1-3 shows percentage increase in diameter for cold-worked and annealed cladding and indicates that cold-worked cladding resulted in less increase. The indications are tempered somewhat by the fact that initial diameter readings were not located so postirradiation values cannot be compared point by point. Nonetheless, the trend appears valid. This is further emphasized by the data plotted in Figure A.1-4 showing percent strain (actually $\Delta d/d$) versus burnup or cold-worked and annealed cladding from the Mark IB subassembly.

The Mark II subassembly consisted of all M316 cold-worked cladding. The pattern of diameter increase was much more consistent in this subassembly than in the previous ones. There were two separate and distinct sets of data results from this subassembly. The interior pins were somewhat hotter than the peripheral pins and experienced higher cladding strain. The range of strains was around 0.8% diametral increase for interior pins and around 0.5% diametral increase for the peripheral pins. These strains were associated with a peak burnup of 59,400 MWd/tonne in the subassembly.

For the Mark IIA subassembly, Figures A.1-5 and A.1-6 respectively, show diameter change versus position along the fuel pin for solution annealed and cold-worked cladding. Coolant flow is downward in the DFR resulting in a temperature profile hotter at the bottom than at the top. It should be noted that the plenum starts at about the 11 in. position. It is readily observed from these plots that the diametral increase for solution treated cladding is substantially greater than for the cold-worked cladding, except at the spacer braze area, about 2 in. from the bottom. However, it must be remembered that this area represents a solution annealed condition.

The conclusion from this British experience is that cold-worked cladding has performed better than solution-annealed to the indicated irradiation levels and temperatures.

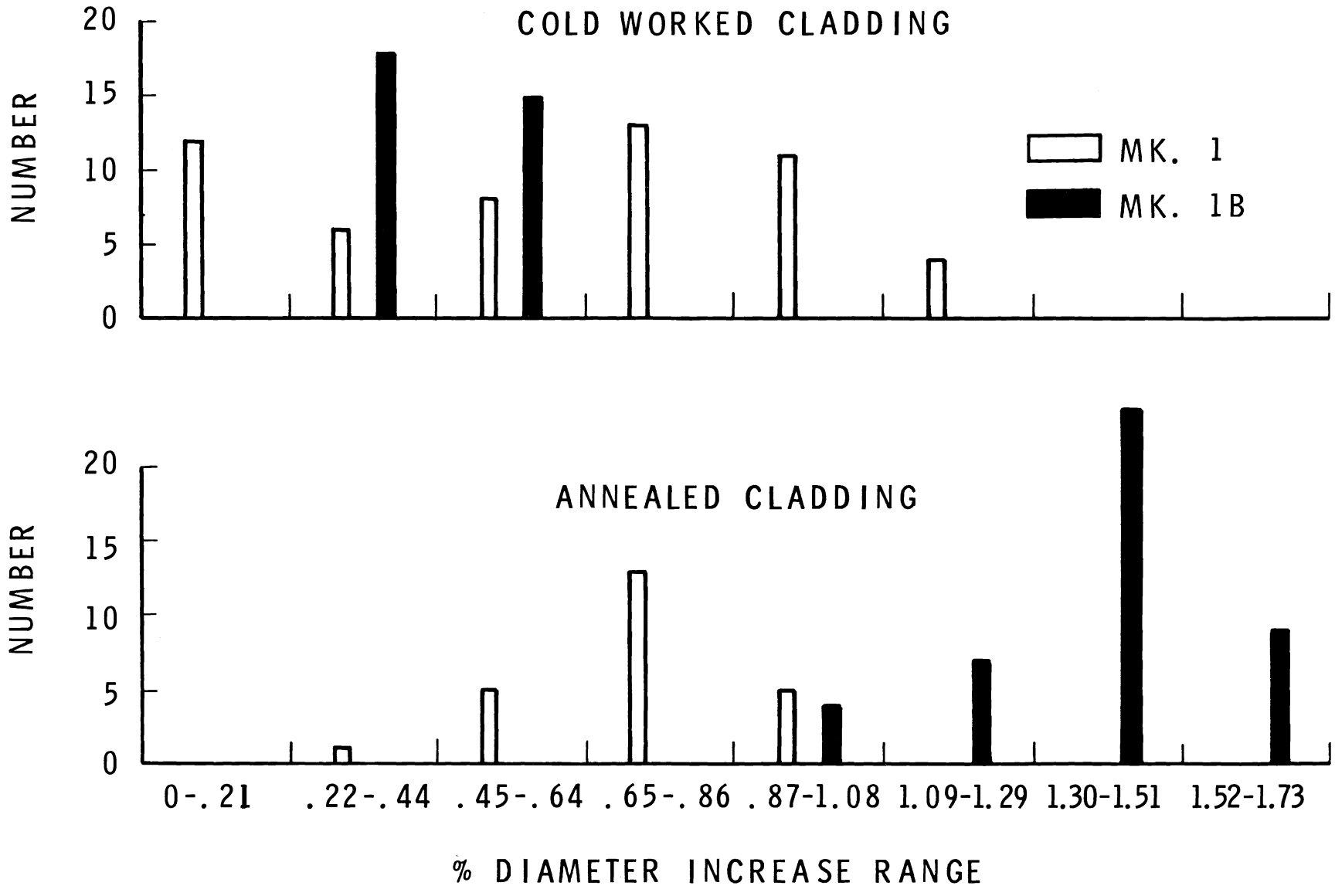

FIGURE A.1-3. Histogram for Mark I and Mark IB of % Diameter Change

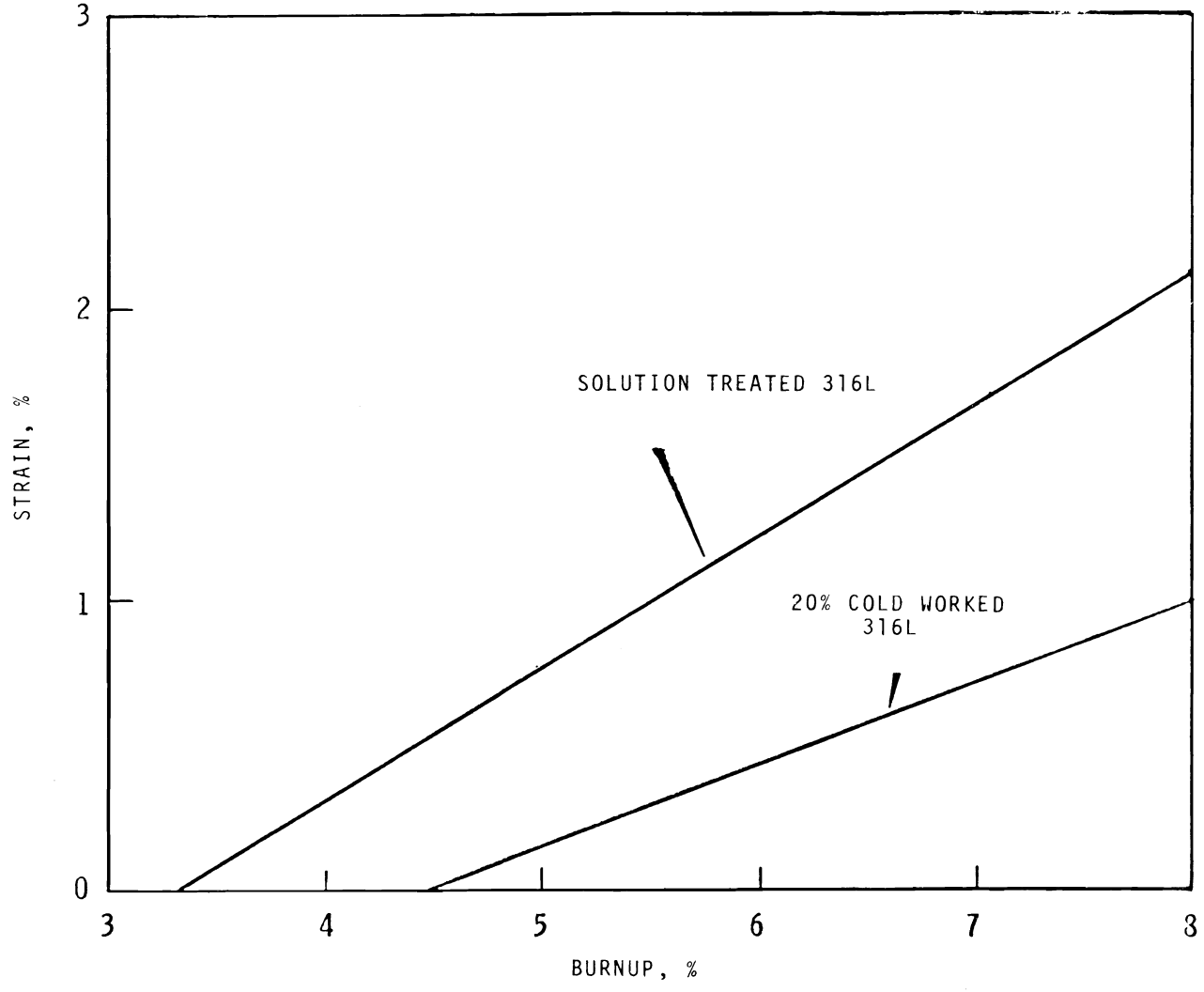

FIGURE A.1-4. Typical Strain/Burnup Relationships at 550 °C for 316L Clad PFR Pins (From D.F.R. Mark IB Subassembly Data)

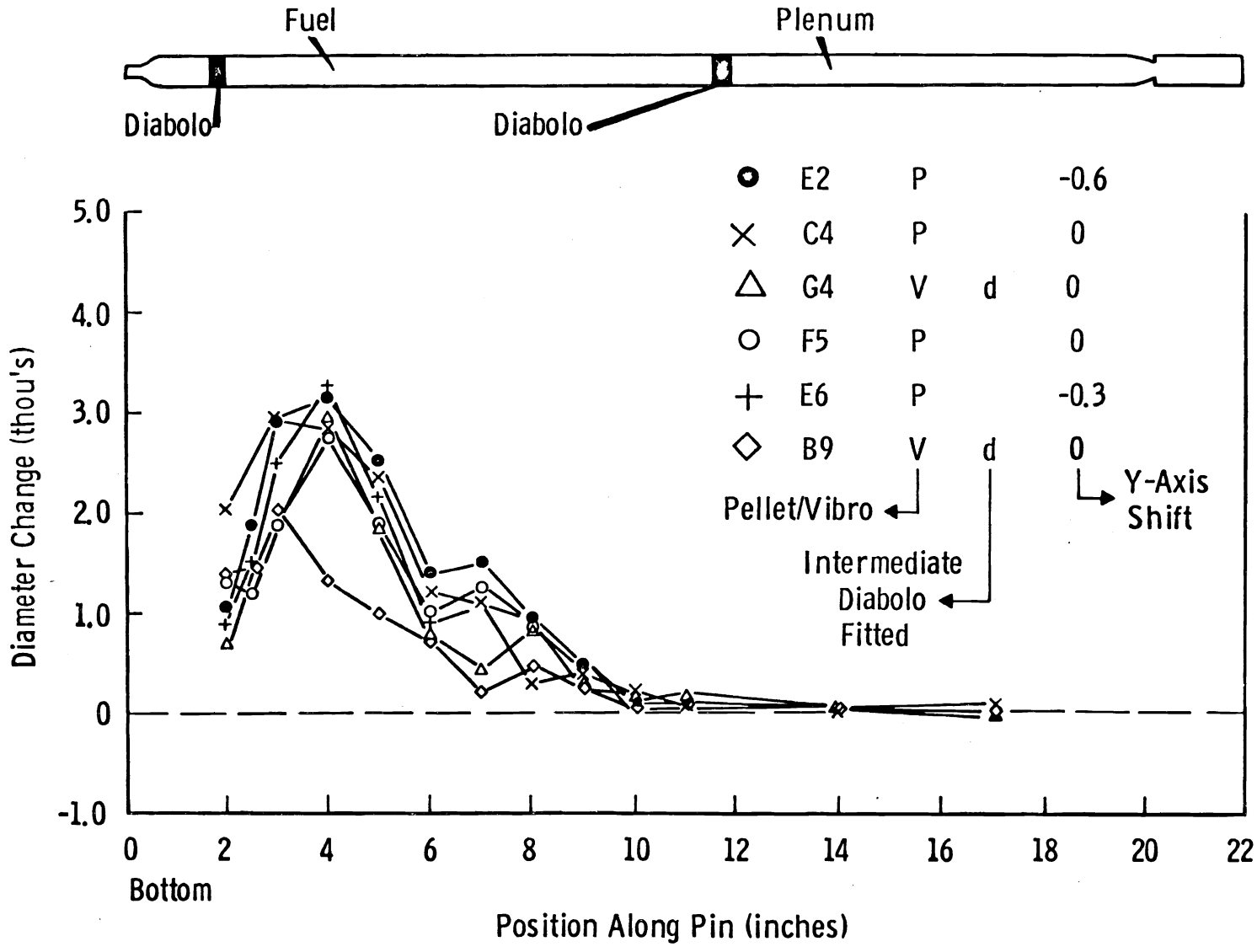

FIGURE A.1-5. Mark IIA Subassembly - Pins with Solution-Treated Clad

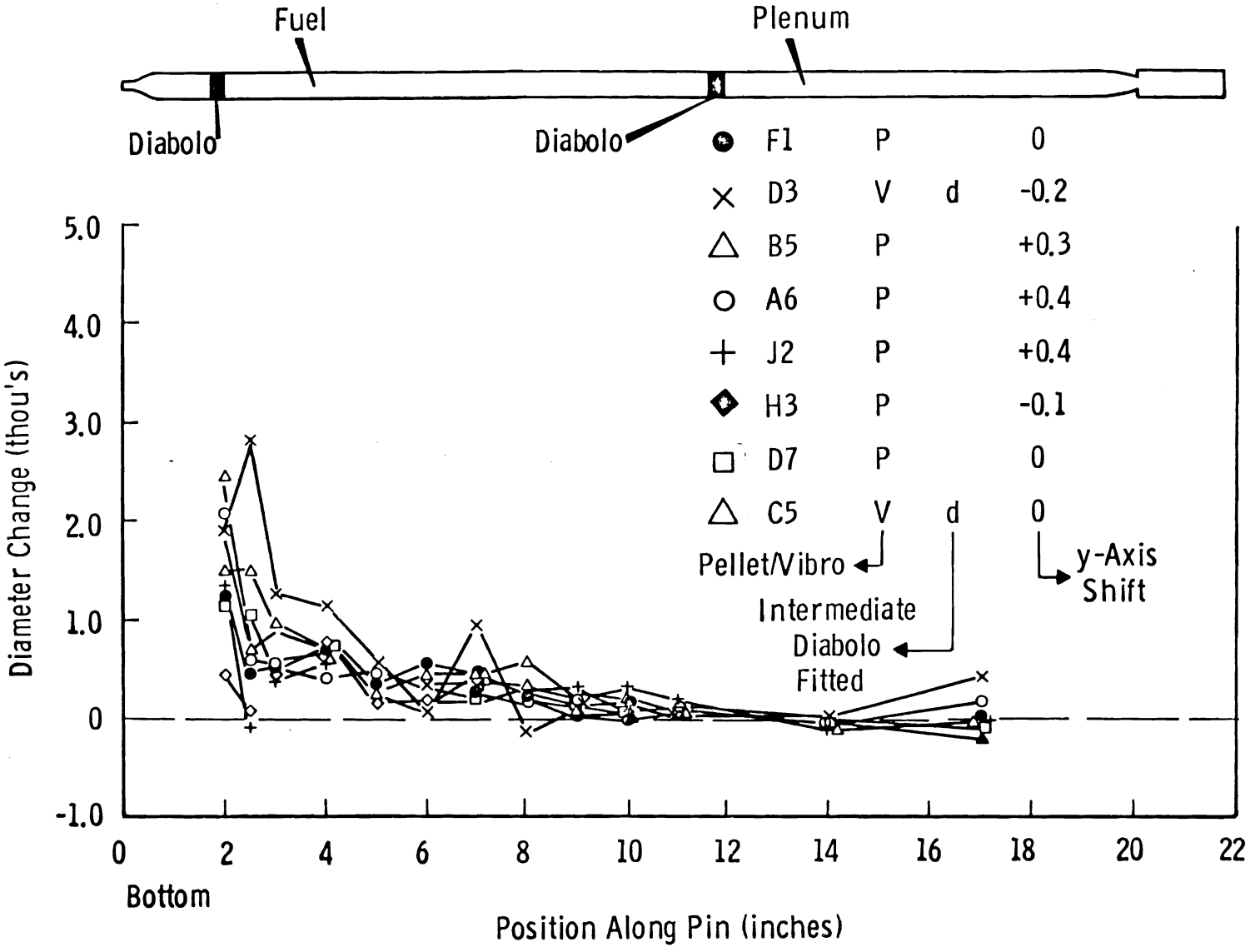

FIGURE A.1-6. Mark IIA Subassembly - Pins with Cold-Worked Clad

A.2 CLAD AND PLENUM SIZING - THERMAL AND PRESSURE STRESS

The fission gas plenum is sized such that it can contain 100% of the fission gas generated in a pin with an average burnup of 64,500 MWd/tonne. This corresponds to 80,000 MWd/tonne peak burnup. The critical parameter is the limited clad ductility for mechanical strain at end-of-life fluence. The allowable stress must be compatible with this ductility.

Clad thickness, clad temperature, and thermal gradients all interact and affect the plenum size required. A slight increase in clad temperature causes a significant increase in creep rate at any particular stress level. Therefore, the allowable stress decreases significantly with a slight increase in clad temperature because of a design limit on mechanical strain. Also, the gas pressure increases with temperature. Increasing the clad thickness decreases the fission gas pressure stress while slightly increasing the thermal stress. The thermal stress in the clad increases with an increased temperature gradient.

A.2.1 Plenum Sizing

The ductility of clad material subject to a total fluence in excess of 10^{23} nvt is expected to be very low. Rupture data obtained on material exposed to a total fluence of about 2×10^{22} nvt indicate that the ductility limit may be approximately 1%. Allowable design stresses are therefore selected to ensure that the maximum clad strains are held to a low level below this value. Applying a strain safety factor of five results in an allowable total strain of 0.2%.

This total strain can have seven separate and distinct components:

1. Elastic Strain
2. Plastic Strain

3. Primary Creep (distinct from Item #2)
4. Secondary Creep
5. Radiation Transient Creep[4,5]
6. Radiation Steady-State Creep[4,5]
7. Thermal Strain.

Items 1 through 6 result from internal fission gas pressure. Item 7 consists of the elastic strain resulting from thermal gradients.

Radiation Enhanced Creep

The radiation enhanced creep is broken down into two components having some similarities to primary and secondary creep. However, the best information available indicates that the radiation transient creep is operative only at fluences between approximately 10^{18} and 10^{20} nvt. Therefore, this would cause creep which would result in relaxation of thermal stress in the clad. However, at these fluences there would be practically no fission gas pressure. As a consequence transient radiation creep has no effect upon plenum design. The radiation steady-state creep appears to be operative only for stresses above 15,000 psi. Because the pressure stress in the plenum is less than this value, the radiation steady-state creep has no effect upon the fission gas plenum design.

Elastic Hoop Strain

The elastic hoop strain in the cylindrical plenum due to pressure of the fission gas is obtained as:

$$\varepsilon_H = \frac{\sigma_H}{E} - \nu\left[\frac{\sigma_A}{E} - \frac{\sigma_R}{E}\right]$$

where

$$\sigma_H = \frac{PRi}{t}$$

$$\sigma_A = \frac{PRi}{2t}$$

$$\sigma_R = \frac{-P}{2}$$

$$\nu = 0.3$$

$$E = 19.32 \times 10^6 \text{ psi at } 650\ ^\circ\text{C}^{(6)*}$$

and

Ri = 0.102 in. (0.002 in. removed from inside of clad due to Fuel-Clad corrosion, scratches, and manufacturing tolerances)

$$t = 0.010 \text{ in.}$$

For a gas pressure of 686.27 psi,

$$\sigma_H = 7{,}000 \text{ psi}$$
$$\sigma_A = 3{,}500 \text{ psi}$$
$$\sigma_R = -343 \text{ psi}$$

Tresca Stress Intensity = 7,000 - (-343) = 7,343 psi

$$\varepsilon_H = 0.031\% \quad .$$

Short Time Plastic Strain

The short time plastic strain exists only if the proportional limit is exceeded. The proportional limit for 316 SS (annealed) at 650 °C is 9,500 psi.[1] Since the effective stress will not reach this limit the short time plastic strain will be zero.

Creep

Both primary and secondary creep are affected by several factors.

1. Biaxiallity
2. Linear increase in stress through life
3. Composition percentages of carbon and nitrogen.

---

* *Table II in Reference 6*

Biaxiallity

The use of "effective" stress ($\bar{\sigma}$) values based on the Von Mises Criterion has been shown[6,7] to be appropriate for creep calculations when biaxial stresses exist.

$$\bar{\sigma} = \sqrt{\frac{1}{2}} \left[(\sigma_1 - \sigma_2)^2 + (\sigma_2 - \sigma_3)^2 + (\sigma_3 - \sigma_1)^2 \right]^{1/2}$$

σ_1, σ_2, σ_3 are the principal stresses.

Principal stresses for the clad wall are obtained as

$$\sigma_H = \frac{PRi}{t}$$

$$\sigma_r = \frac{-P}{2}$$

$$\sigma_A = \frac{PRi}{2t}$$

when

$$\frac{R_i}{t} = \frac{0.102}{0.010} = 10.2$$

$$\bar{\sigma} = \frac{P}{\sqrt{2}} \left[(10.2 + 0.5)^2 + (-0.5 - 5.1)^2 + (5.1 - 10.2)^2 \right]^{1/2}$$

$$\bar{\sigma} = 9.2698P = 0.9088\ \sigma_H$$

Thus the stress biaxiallity reduces the effectiveness of the peak stress in producing creep strain.

The Effect of Pressure Increase with Life

The fission gas buildup in the plenum is assumed to be linear with time. Thus the creep rate early in life will be very low, increasing to a maximum value at the end of the life. The normal representation of minimum (secondary) creep rate is[8]

$$\dot{\varepsilon} = A(\sigma)^B$$

for a creep test a constant stress, $\bar{\sigma}$, the total elongation is:

$$\varepsilon_T^C = \int_o^T \dot{\varepsilon} dt = \dot{\varepsilon} T = A\ (\bar{\sigma})^B T \quad .$$

The linearly increasing stress creep test yields an elongation of ε_T^L at time, T, with a final end-of test stress of σ_o.

$$\sigma = \frac{\sigma_o}{T}\ t$$

$$\varepsilon_T^L = \int_o^T \dot{\varepsilon} dt = \int_o^T A(\sigma)^B dt = \int_o^T A\left(\frac{\sigma_o}{T}\ t\right)^B dt$$

$$\varepsilon_T^L = \frac{A\sigma_o{}^B T}{B+1}$$

The effective constant stress, $\bar{\sigma}$, which provides the same total elongation as the linearly increasing stress test is derived below:

$$\varepsilon_T^L = \varepsilon_T^C$$

which results in

$$\bar{\sigma} = \frac{1}{(B+1)}\left(\frac{1}{B}\right) \times \sigma_o \quad .$$

The ASTM[9] minimum creep rate data on 316 stainless steel at 650 °C yields a value for B of 3.537. Thus:

$$\bar{\sigma} = \frac{\sigma_o}{1.533} = 0.652\ \sigma_o \quad .$$

When the secondary creep rates are calculated, the creep rate for a stress 0.652 times the maximum stress at the end of life will be used. This value will be used as though it existed over the entire life. The applicability of this type of analysis for creep calculations has been verified.[8] Although repeated bursts of primary creep strain were not noted in creep tests under increasing loads, the primary creep strain herein will be calculated using end of life stresses to ensure conservatism.

Effects of Composition

It is known that carbon and other trace elements have a significant effect upon creep and stress rupture behavior of austenitic stainless steel. A recent study[10] of the effects of carbon and nitrogen on 304 SS has concluded that nitrogen is slightly (25%) more effective than carbon in affecting the stress-rupture properties. The approximate composition of industrial 316 SS (i.e., ASTM 122 material) has been estimated to be 0.05% C plus 0.05% N. However, the reference material is expected to contain 0.05% C plus 0.01% N. The referenced material is assumed to have somewhat higher creep rates than normal industrial material. Increasing the primary and secondary creep stress in inverse proportion to the stress to produce rupture in a given time based on the carbon and nitrogen percentages as given by Goodell[10] is considered a conservative means of estimating the effect of composition on the creep strains.

Industrial Material

c = 0.05% N = 0.05% (Estimates)

Parameter = $0.05 + 1.25 \times 0.05 = 0.1125$

$S_{0.1125}$ = 9,000 psi for 10^5 hr. life[10]

Reference Material

C = 0.05% N = 0.01% (Estimates)

Parameter = $0.05 + 1.25 \times 0.01 = 0.0625$

$S_{0.0625}$ = 7,300 psi for 10^5 hr. life.

$K = \frac{9,000}{7,300} = 1.25$

The value of K will be used to increase the stress values (used to calculate primary and secondary creep) to account for the effect of reduced nitrogen level in the reference material as compared to the estimated nitrogen level in industrial material.

Primary Creep Strain

The primary creep strain will be obtained from a linear interpolation of the data reported[6] on M316 material which was 20% cold worked. The following data were extracted from Reference 6:

σ = 7,000 psi , $\varepsilon pc = 0.033\%$

σ = 10,000 psi, $\varepsilon pc = 0.087\%$

Thus the following conservative relationship is assumed.

$$\varepsilon pc = 0.033 + \left(\frac{\sigma - 7,000}{3,000}\right)(0.087 - 0.033) \quad .$$

Consider the following example:

P = 686.27 psi

σ_H = 7,000

accounting for biaxiallity;

$\sigma = 0.9088\ (7,000) = 6,361.6$

accounting for carbon and nitrogen composition;

$\sigma = 1.25\ (6,361.6) = 7,952$ psi

results in $\varepsilon = 0.050\%$ primary creep.

Secondary Creep Strain

The secondary creep rate is taken from the ASTM STP 124[9] data. Biaxiallity, increased load during life, and composition effects are incorporated into the strain calculation.

Consider the following example:

$$P = 686.27 \text{ psi}$$

$$\sigma_H = 7{,}000 \text{ psi}$$

accounting for biaxiallity

$$\sigma = 0.9088\ (7{,}000) = 6{,}362 \text{ psi},$$

accounting for load increase in life

$$\sigma = 0.652\ (6{,}362) = 4{,}148 \text{ psi}$$

accounting for composition

$$\sigma = 1.25\ (4{,}148) = 5{,}185 \text{ psi}$$

thus from Reference 6:

$$\dot{\varepsilon} = 4.7 \times 10^{-8} \text{ in./in./hr.}$$

The secondary creep strain is:

$$T = 1 \text{ yr}, \varepsilon = (4.7 \times 10^{-8})\ (8760)\ (10^2) = 0.041\%$$

$$T = 10^4 \text{ hr}, \varepsilon = (4.7 \times 10^{-8})\ (10^4)\ (10^2) = 0.047\%.$$

Total Strain (Without Thermal ΔT Strain)

The total strain during life is the sum of the six pressure induced components. For the example employed:

$$\varepsilon = 0.031 + 0.0 + 0.050 + 0.047 + 0.0 + 0.0 = 0.128\% \text{ in } 10^4 \text{ hr.}$$

$$\varepsilon = 0.031 + 0.050 + 0.041 = 0.122\% \text{ in 1 yr.}$$

Table A.4-1 gives calculated total strain values for several assumed end of life plenum fission gas pressures.

Ratcheting

The superposition of a radial thermal gradient on the pressure stresses in the plenum may cause ratcheting. Paragraph N-417.3 of Section III of the ASME Boiler and Pressure Vessel Code provides a limit to avoid ratcheting:

$$Y \leq 5.2\ (1 - X)$$

$$X = \frac{\text{Membrane Stress Due to Pressure}}{\text{Yield Strength}}$$

$$Y = \frac{\text{Maximum Range of Thermal Stress}}{\text{Yield Strength}}$$

TABLE A.4-1. Calculation of Total Clad Strains: for 316 SS (20% CW) @ 650 °C

Fission Gas Pressure, psi	Hoop Stress Due to Pressure, psi σ_H	Elastic Hoop Strain, % ε_E	Short Time Plastic Strain, % ε_p	Primary Creep Strain, % ε_{PC}	Secondary Creep Strain In 10^4 hr, % ε_{SC}	Total Strain (w/o thermal) In 10^4 hr, %	Total Strain (w/thermal) In 10^4 hr, %
686.27	7,000	0.031	0.00	0.050	0.047	0.128	0.162
710.29	7,245	0.032	0.0	0.055	0.050	0.137	0.171
738.3	7,531	0.034	0.0	0.061	0.052	0.147	0.181
766.4	7,817	0.035	0.0	0.067	0.060	0.162	0.196
794.4	8,103	0.036	0.0	0.073	0.070	0.179	0.213
831.8	8,484	0.038	0.0	0.080	0.085	0.203	0.237

The maximum ΔT (100 °F) occurs at a location where the clad temperature does not exceed 1100 °F.

The yield strength of 316 SS at 1100 °F should not be less than 12,000 psi.[6,8,9] The limit on thermal stress thus is:

$$\sigma_{Thermal} = 5.2\ (12{,}000) - 5.2\ \sigma_{pressure} .$$

The thermal stress due to a logarithmic thermal distribution is given by Timoshenko.[11]

$$\sigma^{Z}_{Thermal} = \sigma^{\theta}_{Thermal} = \frac{\alpha E \Delta T}{2(1 - \nu)} \left[\log\left(\frac{b}{a}\right) \right]^{-1} \left[1 - \frac{2b^2}{b^2 - a^2} \log \frac{b}{a} \right]$$

b = outside radius = 0.115 in.

a = inside radius = 0.100 in.

$E = 19.32 \times 10^{6}$ psi

$\nu = 0.3$

$\alpha = 10 \times 10^{-6}$ in./in./°F

$$\sigma_{Thermal} = 144.42 \times \Delta T.$$

For a 100 °F ΔT across the clad,

$$\sigma_{Thermal} = 14{,}442 \text{ psi}$$

therefore

$Y = 1.20$

X Allowable = 0.7685

Maximum Membrane Stress = 9,222 psi

Thus, if a ΔT of 100 °F exists, the membrane stress due to pressure must be less than 9,222 psi ($P < 861$ psi) to avoid ratcheting.

Thermal Strain

The ΔT across the clad causes compressive loop (and axial) stresses (and strains) on the inside of the clad. Thus the thermal strain relieves the pressure reduced strains

on the inside of the clad. At the exterior of the clad the thermal stresses (due to the restraint of ΔT growth) cause strains which are additive to the elastic and creep strains resulting from fission gas pressure. The thermal stresses at the outside of the clad are[11]

$$\sigma_\theta = \sigma_Z = \frac{\alpha E \Delta T}{2(1 - \nu) \log \frac{b}{a}} \left[1 - \frac{2a^2}{b^2 - a^2} \log \frac{b}{a}\right]$$

thus

$$\sigma_{Thermal} = 131.58\ \Delta T.$$

However, at the top of the core where the inside of the clad is at 1200 °F the ΔT is only 50 °F, and the resulting thermal strain is:

$$\varepsilon \text{ Thermal} = \frac{131.58\ (50.)}{19.32 \times 10^6} = 0.034\%$$

Table A.4-1 and Figure A.4-1 have entries which include the effect of thermal strain.

Total Strain Including Thermal (ΔT) Strain

Adding the thermal strain (0.034%) to the previously calculated strains results in a total end-of-life strain. The example gives:

$\varepsilon = 0.128\% + 0.034\% = 0.162\%$ in 10^4 hr

$\varepsilon = 0.122\% + 0.034\% = 0.156\%$ in 1 yr.

Table A.4-1 gives the calculated total strain values for several assumed end-of-life plenum fission gas pressures. Figure A.4-1 plots gas pressure versus total calculated end-of-life strain.

Allowable Plenum Pressure

To obtain a total strain at the end of life (including thermal ΔT strain) equal to 0.2%, Figure A.4-1 shows that a fission gas pressure of 772.5 psi must not be exceeded. This pressure avoids ratcheting.

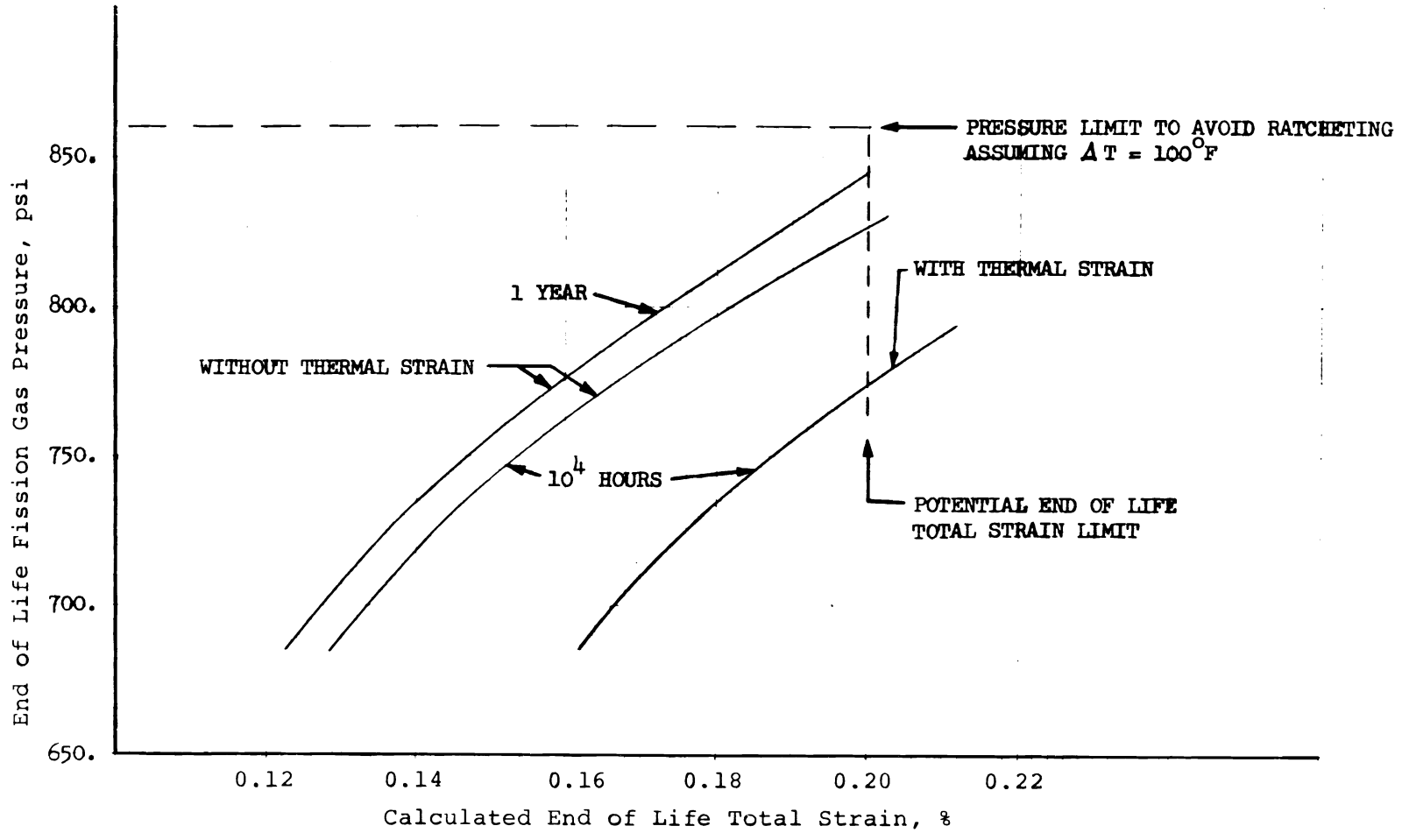

FIGURE A.4-1. Total Strain from Fission Gas Pressure (1200 °F, 316 SS CW)

Fission Gas Pressure

The fission gas plenum pressure was determined by assuming 100 percent of the generated fission gas is released. The peak burnup in the hot rod is 80,000 MWd/tonne with an average burnup of 64,500 MWd/tonne in this rod. The composition of the gases in the plenum include those left in the fuel and plenum during manufacturing as well as the released fission gases. The volume of the various gaseous components are:

Constituent	Amount, cm^3 (a)
Fission Gas (Avg. BU = 64,500 MWd/tonne)	15.67
Water Vapor	7.3
Absorbed Gas	9.7
Helium in Voids	1.1
Helium Back Fill in Plenum	1.0

(a) cm^3 of gas at STP/cm^3 fuel

The resultant pressure from these gases is shown in Figure A.4-2 as a function of effective plenum length. The effective plenum length is defined as the plenum volume divided by the plenum cross sectional area. This is shorter than the actual plenum length because of the internal hardware. From Figure A.4-2 at P = 772.5 psi and maximum clad temperature of 1200 °F the required minimum effective plenum length is determined to be 36.8 in.

Total Plenum Length Calculation

The total plenum volume is:

$$V_T = \pi R_i^2 L_T = \pi (0.1)^2 L_T = 0.031415 L_T \quad .$$

The volume available for gas is

$$V_g = V_T - V_S - V_P - V_{tube}.$$

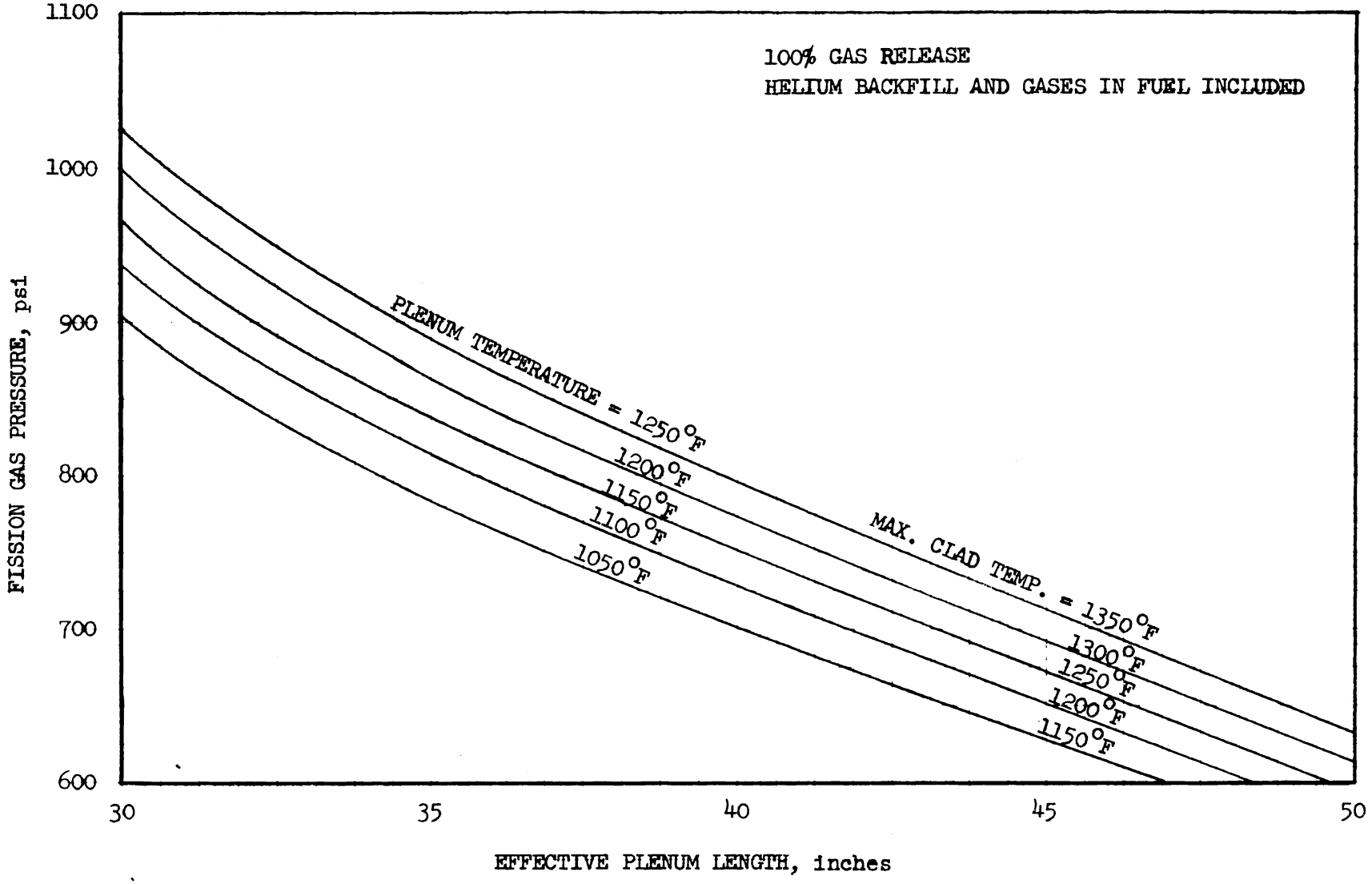

FIGURE A.4-2. Fission Gas Pressure Versus Plenum Length

where

V_S = Volume of spring

V_p = Volume of plug

V_{tube} = Volume of interior tube

V_g = Volume available for gas.

The spring volume is:

$$V_S = N_S \times A_S \times \sqrt{(L_S/N_S)^2 + (\pi D_S)^2}$$

where

N_S = Number of spring coils = 112

A_S = Cross sectional Area of Spring = $\pi (0.0125)^2$
$= 0.00049 \text{ in.}^2$

L_S = Free length of spring = 7 in.

D_S = Coil Diameter (Mean) = 0.187 - 0.025 = 0.162 in.

thus

$$V_S = 112 (0.00049) \sqrt{(0.0625)^2 + (0.5089)^2}$$
$$= 0.02814 \text{ in.}^3$$

The plug volume is:

$$V_p = \frac{\pi (0.192)^2}{4} (0.062) + \frac{\pi (0.154)^2}{4} (0.125) - \frac{\pi (0.062)^2}{4} (0.187)$$

$$V_p = 0.00356 \text{ in.}^3$$

The tube volume is:

$$V_{tube} = L_{tube} \times \frac{\pi}{4} [(0.187)^2 - (0.177)^2] = 0.0028588 \times L_{tube}.$$

The tube length is:

$$L_{tube} = L_T - 6.0 - 0.187 = L_T - 6.187 \text{ in.}$$

Thus, the gas volume is:

$$V_g = 0.031415 L_T - 0.02814 - 0.00356 - 0.0028588 (L_T - 6.187)$$

$$V_g = 0.028557 L_T - 0.014012 \text{ in.}^3$$

The "effective" plenum length = plenum volume/plenum cross sectional area.

$$L_e = \frac{V_g}{A_{plenum}} = \frac{0.028557\ L_T - 0.014012}{0.01\ \pi}$$

Thus for an effective plenum length of 36.8 inches the required real plenum length would be:

$$L_T = \frac{0.01\ \pi\ L_e + 0.014012}{0.028557} = 40.97 \text{ in.}$$

L_T = 41 in.

This design is based upon unirradiated material property data. A basic assumption regarding the allowable strain was made. Assumptions have also been made about the strength effect of changing chemical composition.

In addition there is uncertainty about the effect of in-reactor creep enhancement. Therefore, it is prudent to compare this to design to any available fuel pin performance data.

Table A.4-2 lists pertinent parameters associated with plenum design of selected fuel pins for which no strain occurred in the plenum region. Figure A.4-3 compares these data graphically. It can be noted that the FTR design pressure is somewhat higher than any of the others shown. It is emphasized that no problems occurred with any of these pins. However, because of the lack of experimental justification for the FTR design by operating pins this design must be reviewed in preliminary design.

TABLE A.4-2. Gas Pressure Data Comparison

Identification	Material	Reported Max. Clad Temp, °F	Fission Gas Pressure, psi	Max. or Design Burnup	
				at.%	MWd/tonne
DFR Mark I	M316L ST M316L CW	1060	600	5.5	47,000
DFR Mark IB	M316L ST M316L CW	1120	500	7.0	60,000
DFR Mark IIA	M316 ST M316L CW	1310	200	5.0	42,000
GE XGO 6	316 ST 347 ST Incaloy 800	∿1150	∿500	∿5	∿42,000
RAPSODIE	316	∿1150	680	3.5	∿30,000
FTR	316 CW	1200	772	9.0	80,000

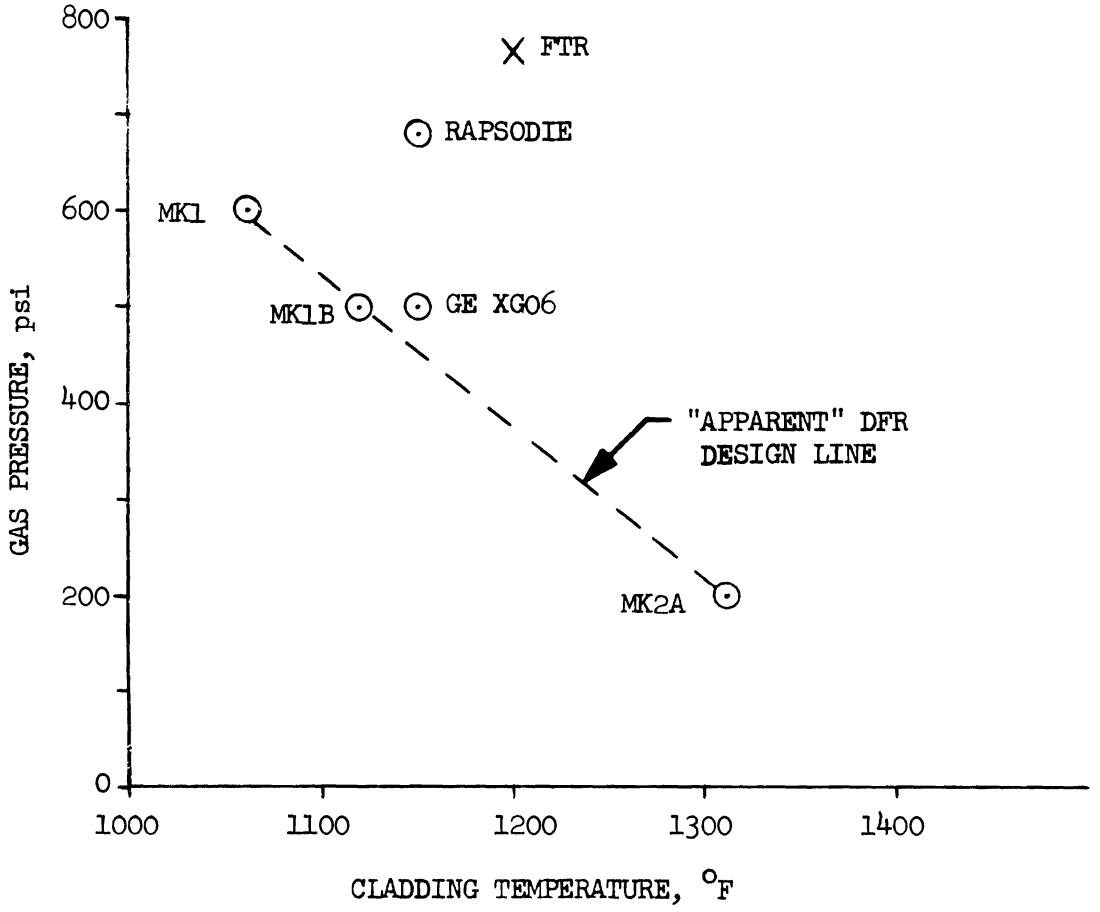

FIGURE A.4-3. Comparison of FTR Gas Plenum Design to Operational Experience

REFERENCES

1. T. T. Claudson and J. E. Irvin. Metallurgical Considerations Affecting the Use of Austenitic Stainless Steel in the Fast Flux Test Facility, BNWL-CC-1004, January 30, 1967. (Unpublished Data)

2. Letter: PNL/FFTF-68954, E. R. Astley to J. M. Shivley, (D. L. Condotta et al.) 9-17-68, FFTF Fuel Cladding Procurement, Attachment B, Evaluation of Cold Working for Type 316 Cladding for FFTF Fuel Pins, T. T. Claudson et al.

3. K. Q. Bagley et al. The Effects of Irradiation in DFR and DMTR on Austenitic Stainless Steels Proposed and P.F.R. Cladding Materials, TRG 1076 (D), (Classified U.K. Commercial), 1966.

4. Memo: P. D. Cohn from R. J. Jackson. Comments on Effect of Duct Swelling and Radiation Creep on FTR Duct Design, December 9, 1968.

5. Memo: J. C. Tobin from R. J. Jackson. Transient Radiation Creep Coefficients, December 9, 1968.

6. A. N. Hughes, A. B. Baldwin and H. Tickle. Interim Report on the Creep and Creep-Rupture Properties of 316 L Type Austenitic Steel, TRG Report 643, (Classified U.K. Commercial), 1963.

7. G. H. Rowe, J. R. Stewart and K. N. Burges. Capped End, Thin Wall Tube Creep Rupture Behavior for Type 316 Stainless Steel, ASME paper 62-Met-7.

8. A. N. Hughes. Creep and Rupture Properties of Potential PFR Cladding Materials: Interim Report, March 1965, TRG-972, (Classified U.K. Commercial).

9. The Elevated Temperature Properties of Stainless Steels, ASTM STP 124, 1952.

10. P. D. Goodell, T. M. Cullen and J. W. Freeman. "The Influence of Nitrogen and Certain Other Elements on the Creep-Rupture Properties of Wholly Austenitic Type 304 Steel," ASME Trans., J. of Basic Engrg., Sept. 1967.

11. S. Timoshenko and J. N. Goodier. The Theory of Elasticity, McGraw-Hill Book Co., Inc., 1951.

DISTRIBUTION

No. of Copies

30 U.S. Atomic Energy Commission
Division of Reactor Dev & Tech
Washington, D.C. 20545

M Shaw, Director, RDT
Asst Dir for Nuclear Safety
Analysis & Evaluation Br, RDT:NS
Environmental & Sanitary Engrg Br, RDT:NS
Research & Development Br, RDT:NS
Asst Dir for Plant Engrg, RDT
Facilities Br, RDT:PE
Components Br, RDT:PE
Instrumentation & Control Br, RDT:PE
Liquid Metal Systems Br, RDT:PE
Asst Dir for Program Analysis, RDT
Asst Dir for Project Mgmt, RDT
Liquid Metals Projects Br, RDT:PM
FFTF Project Manager, RDT:PM (3)
Asst Dir for Reactor Engrg, RDT
Control Mechanisms Br, RDT:RE
Core Design Br, RDT:RE (2)
Fuel Engineering Br, RDT:RE
Fuel Handling Br, RDT:RE
Reactor Vessels Br, RDT:RE
Asst Dir for Reactor Tech, RDT
Coolant Chemistry Br, RDT:RT
Fuel Recycle Br, RDT:RT
Fuel & Materials Br, RDT
Reactor Physics Br, RDT:RT
Special Technology Br, RDT:RT
Asst Dir for Engrg Standards, RDT
Asst Dir for Nuclear Safety, RDT

3 AEC Richland Operations Office
FFTF Program

J. M. Shivley

4 AEC Site Representatives - BNW

P. G. Holsted

43 Battelle-Northwest

E. R. Astley
J. C. Cochran
P. D. Cohn
D. L. Condotta
E. A. Evans
F. C. Gronemeyer
P. L. Hofmann
R. J. Jackson
D. C. Kolesar
W. B. McDonald
C. L. Mohr
A. Padilla
R. J. Squires
E. G. Stevens
C. L. Wheeler
FFTF Files (2)
300 TID File (25)
FFTF Technical Publications Office